Myeloid-derived suppressor cell dynamics control outcomes in the metastatic niche

Jesse Kreger[a], Evanthia T. Roussos Torres[b], Adam L. MacLean[a,*]

[a]Department of Quantitative and Computational Biology, University of Southern California, 1050 Childs Way, Los Angeles, CA 90089, USA

[b]Norris Comprehensive Cancer Center, Keck School of Medicine, University of Southern California, 1441 Eastlake Ave, Los Angeles, CA 90033, USA

[*]macleana@usc.edu

Abstract

Myeloid-derived suppressor cells (MDSCs) play a prominent and rising role in the tumor microenvironment. An understanding of the tumor-MDSC interactions that influence disease progression is critical, and currently lacking. To address this, we developed a mathematical model of metastatic growth and progression in immune-rich tumor microenvironments. We model the tumor-immune dynamics with stochastic delay differential equations, and study the impact of delays in MDSC activation/recruitment on tumor growth outcomes. We find when the circulating level of MDSCs is low, the MDSC delay has a pronounced impact on the probability of new metastatic establishment: blocking MDSC recruitment can reduce the probability of metastasis by as much as 50%. We also quantify the extent to which decreasing the immunosuppressive capability of the MDSCs impacts the probability that a new metastasis will persist or grow. In order to quantify patient-specific MDSC dynamics under different conditions we fit individual tumors treated with immune checkpoint inhibitors to the tumor-MDSC model via Bayesian parameter inference. We reveal that control of the inhibition rate of natural killer cells by MDSCs has a larger influence on tumor outcomes than controlling the tumor growth rate directly. Posterior classification of tumor outcomes demonstrates that incorporating knowledge of the MDSC responses improves predictive accuracy from 63% to 82%. Our results illustrate the importance of MDSC dynamics in the tumor microenvironment and predict interventions that may shift environments towards a less immune-suppressed state. We argue that there is a pressing need to more often consider MDSCs in analyses of tumor microenvironments.

1 Introduction

Myeloid-derived suppressor cells (MDSCs) are immature myeloid immune cells that become pathologically activated with potent immunosuppressive activity (1–7). Since the introduction of the term "MDSC" in the late 1990s (4–6), there has a great deal of effort to understand MDSC phenotypes and dynamics. MDSCs are implicated in the regulation of immune responses in many biological contexts and pathological conditions, including cancer, inflammation, wound healing, and autoimmune disorders (1). Some have gone as far as to claim that MDSCs are "the most important cell you have never heard of" (8). Recently, with the advent of high-dimensional measurement technologies including mass cytometry and single-cell RNA sequencing, the characterization of MDSCs and their roles in diverse contexts has become more refined (7, 9). Here, we characterize MDSCs by their function – immunosuppressive activity – rather than their expression phenotype (e.g. $CD11b^+$ and $Gr\text{-}1^+$ in mice), bypassing the need to delve into the heterogeneity of the $CD11b^+Gr\text{-}1^+$ population at single-cell level.

In the context of cancer, the role of MDSCs is convoluted, in part due to the complexity of the tumor microenvironment and related immunology (3, 10–14). MDSCs certainly play significant roles in tumor microenvironments (8, 9, 15, 16); increased levels of MDSCs are associated with poor clinical outcomes (2, 12, 17–19) (An important caveat is that studies often measure only circulating MDSCs.) There is compelling evidence that MDSCs can effectively shield tumors from anti-tumor immune responses from cytotoxic T cells and natural killer cells (20–24). Targeting MDSCs as a way to sensitize non-immunogenic tumors is an attractive treatment strategy in cancer immunotherapy (16, 17). MDSC dynamics have also been studied in the specific context of breast cancer, where they have been shown to affect the progression of primary breast tumors and associated metastases (7, 15, 18, 23, 25–27).

Understanding tumor-immune-MDSC dynamics is by nature a systems biology problem. Mathematical and computational modeling are essential to tease apart the intricate relationships involved (28, 29). There have been relatively few works (certainly in comparison to experimental/clinical interest) in the literature that develop mathematical models of MDSCs (30–33). Shariatpanahi et al. (30) developed a model described by ordinary differential equations with which they explore therapeutic strategies that aim to restore anti-tumor immunity, in comparison with experimental data (23). Allahverdy et al. (31) developed a stochastic agent-based model was used to explore the effects of different drugs on MDSC and tumor dynamics. Liao et al. (32, 33) developed a model described by partial differential equations were used to determine optimized drug treatment and to understand primary drug resistance. While these models offer insight into the roles of MDSCs, a rigorous treatment of MDSC dynamics in the tumor microenvironment, fitting models to data, and taking into account the effects of noise remains lacking.

Here, we focus on the effect of MDSC dynamics on metastatic tumor growth following an initial seeding event. A majority of cancer deaths are a result of metastasis (34): a highly dynamic and stochastic process. Most metastatic tumors are seeded by a small number of circulating tumor cells (13, 34). MDSC migration to the site of a new tumor has been identified as crucial for cancer progression, both in primary tumors and metastases, but the interactions involved are not well understood, in part due to the novelty of MDSC characterization, the complex tumor-immune environment, and the difficulties associated with tracking cell-cell interactions *in vivo* (13, 35, 36). As a result, there are many open and pressing questions regarding MDSCs and tumor metastasis (37). How much therapeutic benefit can be gained by blocking MDSC recruitment to the tumor site? Would therapies that decrease the circulating number of MDSCs achieve similar or greater effects? There are now various methods to target MDSCs in peripheral lymphoid organs and their migration to tumor sites. However, it is not clear whether either of these methods alone will be sufficient to inhibit MDSC immunosuppressiveness at a tumor site or whether combination approaches will be required.

To address these questions we develop a stochastic delay differential equation model of metastatic

tumor growth. We include an MDSC delay that can represent delays in MDSC recruitment to the metastatic tumor site as well as delays in MDSC activation to suppress anti-tumor immune cells. Stochasticity is included due to the inherent noise in the cell dynamics, and to be able to assess the probabilistic events of new metastases. We first demonstrate the importance of MDSCs in the tumor-immune microenvironment, and establish conditions necessary for metastatic growth for the deterministic model. We then identify the most important parameters and interactions in the system, to shed light on the underlying biological dynamics. Next, through simulation we explore the impact of MDSC delays on metastatic growth, we discover that under certain conditions inhibiting MDSC recruitment alone might be a highly effective treatment strategy. Finally, we perform Bayesian parameter estimation of models fit to individual tumors growing *in vivo*, from which we determine tumor- and MDSC-specific parameters. Inference results reveal that knowledge of MDSC-specific parameters is important in order to be able to accurately predict metastatic outcomes.

2 Methods

2.1 A stochastic delay differential equation model of tumor-immune dynamics in the presence of MDSCs

Mathematical modeling of tumor-immune cell interactions has been increasingly recognized as critical for understanding strategies to mount an effective response to cancer initiation, spread, and evolution (28, 29, 38–43). In this paper we first describe a theoretical basis for MDSC dynamics in the context of a metastasizing tumor (e.g. in the lung, bone, or liver (44)) from a primary tumor in the breast. For parameterization of the model, we focus on the lung, as it is one of the most common distant metastases sites of breast cancer (45). Our mathematical model is comprised of four non-spatial delay differential equations to describe tumor-immune interactions incorporating MDSCs (30, 40). We focus on the most important interactions between tumor, immune, and MDSC populations, leading to a relatively simple model that allows us to gain insight into system dynamics and metastatic tumor spread. We include the anti-tumor immune populations of cytotoxic T (CTL) cells and natural killer (NK) cells. MDSC-CTL interactions are important given the primary function of intratumoral MDSCs is suppression of CTLs (1, 6, 15, 16). MDSC-NK interactions are also important (20–22, 24, 25), and NK cells are increasingly being studied as an immune population specifically affected by tumor cells to promote metastasis (46, 47). A schematic diagram of the model is provided in Figure 1.

We denote x_{T}, x_{MDSC}, x_{NK}, and x_{CTL} as the populations of tumor cells, MDSCs, NK cells, and CTL cells, respectively, at time t. The model derived can be expressed conceptually (i.e. agnostic as yet to the form of the dynamics) as follows, where δx_i denotes the rate of change of x_i, $i \in$ [T, MDSC, NK, CTL].

$$\begin{aligned}
\delta x_{\mathrm{T}} &= \boxed{\text{growth of tumor cells}} - \boxed{\text{tumor cells inhibited by NK cells}} \\
&- \boxed{\text{tumor cells inhibited by CTL cells}} - \boxed{\text{death of tumor cells}}, && \text{(1a)} \\
\delta x_{\mathrm{MDSC}} &= \boxed{\text{circulating level of MDSCs}} + \boxed{\text{recruitment of MDSCs in presence of tumor}} \\
&- \boxed{\text{death of MDSCs}}, && \text{(1b)} \\
\delta x_{\mathrm{NK}} &= \boxed{\text{circulating level of NK cells}} + \boxed{\text{recruitment of NK cells in presence of tumor}} \\
&- \boxed{\text{NK cells inhibited by MDSCs}} - \boxed{\text{death of NK cells}}, && \text{(1c)} \\
\delta x_{\mathrm{CTL}} &= \boxed{\text{CTL cells stimulated by NK-tumor interaction}} + \boxed{\text{recruitment of CTL cells in presence of tumor}} \\
&- \boxed{\text{CTL cells inhibited by MDSCs}} - \boxed{\text{death of CTL cells}}, && \text{(1d)}
\end{aligned}$$

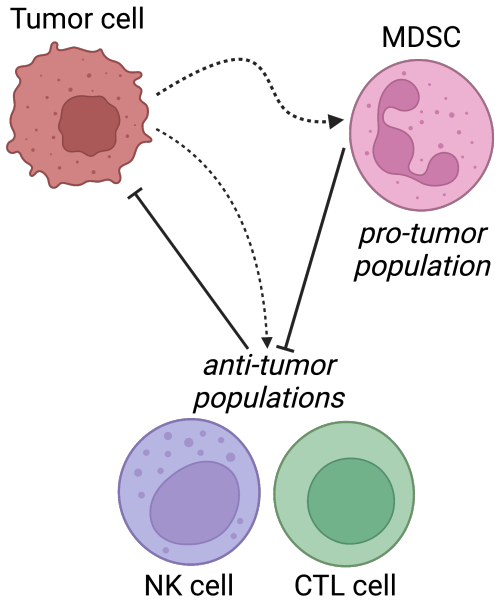

Figure 1: **Schematic diagram of model and population interactions.** The myeloid-derived suppressor cell (MDSC), natural killer (NK) cell, and cytotoxic T (CTL) cell populations are all signaled to proliferate in the presence of a metastatic tumor. The MDSC population inhibits the NK and CTL populations, and the NK and CTL populations inhibit the tumor population.

Based on these biological processes, we develop a stochastic delay differential equation (SDDE) model to characterize tumor-immune interactions that takes the form:

$$dx_i(t) \quad = \quad f(x_{\mathbf{j}}(t), x_{\mathbf{j}}(t-\tau))dt + g(x_{\mathbf{j}}(t), x_{\mathbf{j}}(t-\tau))dW(t), \tag{2}$$

at time t, with delay $0 < \tau < t$, where $f(\cdot)$ describes the deterministic dynamics controlled by the model interactions, $g(\cdot)dW(t)$ describes the stochastic dynamics, $dW(t)$ denotes an increment of a Weiner process, $W(t)$, and $x_{\mathbf{j}}(t) = [x_{\mathrm{T}}(t), x_{\mathrm{MDSC}}(t), x_{\mathrm{NK}}(t), x_{\mathrm{CTL}}(t)]$. The model thus consists of coupled stochastic delay differential equations (SDDEs), where we assume an Itô interpretation (48). For the stochastic dynamics, we have:

$$g(x_{\mathbf{j}}(t), x_{\mathbf{j}}(t-\tau)) = \xi_i(t),$$

where $\xi_i(t)$ is the size of the i^{th} population, i.e. we assume multiplicative noise (48, 49). We study the tumor-immune dynamics under the assumption of multiplicative noise given the mounting evidence that biological systems more often exhibit dynamics generated from multiplicative noise models (50).

For the deterministic dynamics, we have:

$$f(x_{\mathbf{j}}(t), x_{\mathbf{j}}(t-\tau)) = \begin{bmatrix} \alpha_1 x_{\mathrm{T}}(t) \log\left(\dfrac{\eta}{x_{\mathrm{T}}(t)}\right) - \beta_1 x_{\mathrm{T}}(t) x_{\mathrm{NK}}(t) - \beta_2 x_{\mathrm{T}}(t) x_{\mathrm{CTL}}(t) - \zeta_1 x_{\mathrm{T}}(t) & \text{(3a)} \\ \alpha_2 + \alpha_3 \dfrac{x_{\mathrm{T}}(t-\tau)}{\gamma_1 + x_{\mathrm{T}}(t-\tau)} - \zeta_2 x_{\mathrm{MDSC}}(t) & \text{(3b)} \\ \alpha_4 + \alpha_5 \dfrac{x_{\mathrm{T}}(t)^2}{\gamma_2 + x_{\mathrm{T}}(t)^2} - \beta_3 x_{\mathrm{MDSC}}(t) x_{\mathrm{NK}}(t) - \zeta_3 x_{\mathrm{NK}}(t) & \text{(3c)} \\ \alpha_6 x_{\mathrm{T}}(t) x_{\mathrm{NK}}(t) + \alpha_7 \dfrac{x_{\mathrm{T}}(t)^2}{\gamma_3 + x_{\mathrm{T}}(t)^2} - \beta_4 x_{\mathrm{MDSC}}(t) x_{\mathrm{CTL}}(t) - \zeta_4 x_{\mathrm{CTL}}(t) & \text{(3d)} \end{bmatrix},$$

with description of the parameters is given in Table 1. We model tumor growth according to a Gompertzian model (first term of Eqn. (3a)) (30, 38), with maximum size η, where tumor cells can

be eradicated by the NK and CTL cells (anti-tumor response), with rates β_1 and β_2, respectively. MDSCs are activated due to their basal circulation, α_2, and die at rate ζ_2. In addition, in the presence of tumor cells, immune-suppressive signals lead to increased MDSC production, activation, and recruitment to the site of the tumor (at rate α_3). MDSCs, generated primarily in the bone marrow, migrate to peripheral lymphoid organs and then to tumor tissues in tumor bearing hosts (13, 51). The delay in activation/recruitment of MDSCs is modeled using a Mackey-Glass delay term (52), with a delay of order τ (second term of Eqn. (3b)). Here we consider delays only in x_{MDSC}; while delays in other immune cells, e.g. due to CTL activation, might be important in some contexts, they were observed to have small effects on the tumor dynamics here, due to the low circulating levels of CTL cells (see Supplementary Text Section 1). We also note that the model does not include MDSC subtypes or maturation, but only accounts for their functional significance as immature myeloid cells with immunosuppressive capability. Future work could include MDSC maturation into other cell types as influenced by the tumor microenvironment, see the Discussion for further details.

For the anti-tumor immune dynamics, NK cells are produced at rate α_4; CTL cells are activated by the NK cell—tumor cell interaction at rate α_6. In line with (30), both NK and CTL cells can be activated by the tumor (at rates α_5 and α_7, respectively). We assume that NK and CTL cells can be inhibited by MDSCs (at rates β_3 and β_4, respectively), and are lost due to cell death (at rates ζ_3 and ζ_4, respectively). In simulations of new metastases (with Eqns. (3a)-(3d)), the initial conditions are set by the tumor-free steady state (Eqns. 5b)-(5d)), except that we seed tumor growth by one or two initial tumor cells. Unless explicitly stated otherwise, all parameter values used for simulation are as defined in Table 1. The standard error is defined as standard deviation/$\sqrt{\text{number of simulations}}$. The red lines represent the tumor population, the yellow lines represent the MDSC population, the green lines represent the NK cell population, and the blue lines represent the CTL population. The horizontal axis is the time in days, and the vertical axis is the size of the population (see for example Figure 2).

In our studies below we consider analyses of the full SDDE model as well as different reduced models. In the case that $g = 0$, the SDDE model reduces to a deterministic delay differential equation (DDE) model. In the case that $g = 0$ and $\tau = 0$, the model reduces to an ordinary differential equation (ODE) model. All models are developed in the Julia programming language (53), using DifferentialEquations.jl (54). For simulation of the full model, we use the SOSRI algorithm for stiff stochastic differential equations (55). Metaprogramming in Julia enables transitioning between model formulations (SDDE, DDE, or ODE) with ease (56).

2.2 Parameter sensitivity analysis

We perform parameter sensitivity analysis to assess the relative importance of parameters on the model given by Eqns. (3a)-(3d). We use Morris global sensitivity analysis (GSA) (66, 67) for the steady state of the tumor population for all model parameters. Table 1 contains GSA ranges and parameter descriptions. The parameters used for the Morris algorithm (using DifferentialEquations.jl (54)) are $total\_num\_trajectory = 1000$ and $num\_trajectory = 100$.

2.3 Bayesian parameter inference with RECIST data

RECIST criteria have been developed for use in clinical trials as a way to determine the change in tumor burden of selected target lesions to inform whether a patient is responding to a given therapy (68). We implement Bayesian parameter inference to fit the model to tumor responses using RECIST to classify tumor sizes and responses over time (described below, (69)). We fit differential equation-based models to RECIST data following a similar conceptual framework to (38). In the case of our model, we also fit certain MDSC parameters, such as the interaction strengths between the MDSCs and other immune/tumor populations, to assess the effect of MDSC dynamics on

Notation	Description	Value	Units	Reference	Range
$x_{\mathrm{T}}(t), t \leq 0$	initial condition for tumor cells	1 or 2	-	-	-
$x_{\mathrm{MDSC}}(0)$	initial condition for MDSCs	α_2/ζ_2	-	-	-
$x_{\mathrm{NK}}(0)$	initial condition for NK cells	$\frac{\zeta_2\alpha_4}{\alpha_2\beta_3+\zeta_2\zeta_3}$	-	-	-
$x_{\mathrm{CTL}}(0)$	initial condition for CTL cells	0	-	-	-
τ	delay parameter for MDSCs	varies	days	-	-
α_1	tumor growth rate	10^{-1}	days^{-1}	(40, 57, 58)	$[10^{-2}, 5\times10^{-1}]$
η	tumor maximum size	10^7	-	estimated	$[10^6, 10^8]$
β_1	tumor cells inhibition rate by NK cells	3.5×10^{-6}	days^{-1}	(40, 57, 58)	$[10^{-7}, 10^{-6}]$
β_2	tumor cells inhibition rate by CTL cells	1.1×10^{-7}	days^{-1}	(57)	$[10^{-7}, 10^{-6}]$
ζ_1	tumor cell death rate	0, varies	days^{-1}	(30)	$[0, 0.1]$
α_2	MDSCs circulating rate	10^2, varies	days^{-1}	estimated (59)	$[0, 10^3]$
α_3	MDSCs expansion coefficient	10^8	days^{-1}	(23, 30, 60, 60)	$[10^7, 10^9]$
ζ_2	MDSCs death rate	0.2	days^{-1}	(61, 62)	$[0, 1]$
α_4	NK cells circulating rate	1.4×10^4	days^{-1}	(57)	$[10^3, 10^5]$
α_5	NK cells expansion coefficient	2.5×10^{-2}	days^{-1}	(40, 57, 58)	$[10^{-2}, 10^{-1}]$
β_3	NK cells inhibition rate by MDSCs	4×10^{-5}, varies	days^{-1}	(30)	$[10^{-5}, 10^{-4}]$
ζ_3	NK cells death rate	4.12×10^{-2}	days^{-1}	(57)	$[10^{-2}, 10^{-1}]$
α_6	CTL stimulation by tumor-NK cell interaction	1.1×10^{-7}	days^{-1}	(63, 64)	$[10^{-7}, 10^{-6}]$
α_7	CTL expansion coefficient	10^{-1}	days^{-1}	(65)	$[5\times10^{-2}, 10^{-1}]$
β_4	CTL inhibition rate by MDSCs	10^{-4}, varies	days^{-1}	(30)	$[5\times10^{-5}, 5\times10^{-4}]$
ζ_4	CTL death rate	2×10^{-2}	days^{-1}	(40, 63)	$[10^{-2}, 10^{-1}]$
γ_1	steepness of MDSC production	10^{10}	-	(30, 60)	$[10^9, 10^{11}]$
γ_2	steepness of NK production	2.02×10^7	-	(40, 57)	$[10^6, 10^8]$
γ_3	steepness of CTL production	2.02×10^7	-	(40, 57, 58)	$[10^6, 10^8]$

Table 1: **Description of model parameters and values.** Estimated from the literature, see in particular (40, 57, 59, 60). Cell populations are measured in terms of cell numbers and are non-dimensionalized. The first column is the parameter notation, the second column is the parameter description, the third column is the parameter estimated value, the fourth column is the parameter units (if applicable), the fifth column is the citation of the reference for the parameter estimate, and the sixth column is the parameter range used for the global stability analysis in Section 3.2.

clinically-relevant tumor growth. We employ Bayesian parameter inference (70) implemented in Turing.jl (71).

We use *in vivo* tumor data from a study evaluating the efficacy and safety of anti-programmed death-ligand 1 (PD-L1) atezolizumab in advanced non-small cell lung cancer (69). This data was also recently used to fit mathematical models of tumor growth (Study 1, (38)). Each tumor has a baseline assessment before the initiation of treatment in the clinical trial (for the purposes of fitting we set the time of the baseline assessment to be zero). Tumor size is then reassessed approximately every six weeks for twelve months, then every nine weeks, and then at disease progression. At each assessment the tumor size is measured in millimeters in one dimension (x), which we convert to a volume following the convention adopted by Laleh et al., i.e. taking the volume (mm^3) as $\frac{1}{2}x^3$ (38, 72). We estimate the number of tumor cells from this volume by multiplying by a factor of 10^7 (73). From the available data we selected six measurable tumors from six different patients that each have data from at least five time points (including the baseline assessment), are from all three study cohorts, and are representative of the range of the dataset (i.e. tumors that increase/decrease at a variety of rates). We fit the *relative change* in the tumor population, which is measured as the difference between the measurement and the baseline assessment, divided by the baseline assessment ($\frac{\text{measurement}-\text{baseline}}{\text{baseline}}$, which produces a real number $\in [-1, \infty)$). As the relative change at the baseline assessment is always zero, we remove this data point for all tumors. Since only the tumor data is available, we fit the log transformed data from this population (i.e. $\log(x_{\mathrm{T}}+1)$). All of the data for each of the six tumors is available in the supplementary file tumor_data.xlsx.

For inference, a three-dimensional free parameter space was selected in which we fit the following parameters: β_3 (NK cells inhibition rate by MDSCs), α_6 (CTL stimulation by tumor-NK cell interaction), and α_1 (tumor growth rate). As no information on time since incidence was available, we set the initial conditions according to previous simulations (see Figure 2A and Table 1) at day

100 ($x_{\mathrm{T}}(0) = 8395.4$, $x_{\mathrm{MDSC}}(0) = 804.1$, $x_{\mathrm{NK}}(0) = 197565.7$ and $x_{\mathrm{CTL}}(0) = 1654.4$). Therefore, we rescale $\eta = 10^5$ (tumor maximum size), and all other parameters are set to be as in Table 1 with $\tau = 0$. The weakly informative prior distributions for the parameters (means set to the values in Table 1 and the standard deviations set to be wide) for the Bayesian parameter estimation are as follows:

$$\begin{aligned}
\beta_3 &\sim \text{truncated}\left(\mathcal{N}\left(4\times10^{-5}, 10^{-4}\right), 0, 10^{-2}\right) && \text{(4a)}\\
\alpha_6 &\sim \text{truncated}\left(\mathcal{N}\left(1.1\times10^{-7}, 10^{-6}\right), 0, 10^{-2}\right) && \text{(4b)}\\
\alpha_1 &\sim \text{truncated}\left(\mathcal{N}\left(10^{-1}, 3\times10^{-1}\right), 0, 1\right) && \text{(4c)}\\
\sigma &\sim \text{InverseGamma}\left(2, 3\right) && \text{(4d)}
\end{aligned}$$

where σ is the noise estimate. For each tumor we run four independent Markov chain Monte Carlo (MCMC) simulations with 2×10^3 iterations using the No U-Turn Sampler (NUTS) with a target acceptance ratio of 0.65 (74).

2.4 Decision tree classification of tumor responses

We train decision trees classifiers on different combinations of posterior parameters from the Bayesian parameter inference to classify tumor response as either decreasing or increasing over time. Decision trees are built using DecisionTree.jl (75) and cross validation is done using scikit-learn (76).

3 Results

3.1 Dynamics of metastatic growth in the presence of MDSCs

We study MDSC dynamics in the context of a metastasizing tumor, specifically we focus on breast-to-lung metastasis, i.e. metastatic growth in the lung resulting from a primary tumor in the breast. Thus to parameterize the model, we take into account the immune cell composition known to be present in tumors in lungs (77) (Figure 1). We begin by analyzing the behavior of the deterministic model (delay differential equations (DDEs); Eqns. (3a)-(3d, $g = 0$). Simulation of the DDE model for different sizes of MDSC delay (τ) show that the delay in the recruitment of MDSCs to the tumor site plays a critical role in determining metastatic tumor size after one year (Figure 2). We see that increasing τ leads to slower growth and smaller population sizes of both the MDSC and tumor populations. Increasing the delay leads to a lag before the MDSCs receive activation signals from the tumor and begin to proliferate. Smaller MDSC population sizes lead to slower growth/smaller tumor population sizes because a smaller MDSC population makes the tumor more immunosusceptible to cell killing by NK and CTL populations. Note that, given the parameters in Table 1, the same steady state will be reached for any finite τ, $0 \leq \tau < \infty$. The time until steady state is positively correlated with the delay τ.

In the case of no tumor ($x_{\mathrm{T}} = 0$), the tumor-free fixed point of the model is:

$$\begin{aligned}
\hat{x}_{\mathrm{T}} &= 0, && \text{(5a)}\\
\hat{x}_{\mathrm{MDSC}} &= \frac{\alpha_2}{\zeta_2}, && \text{(5b)}\\
\hat{x}_{\mathrm{NK}} &= \frac{\zeta_2\alpha_4}{\alpha_2\beta_3 + \zeta_2\zeta_3}, && \text{(5c)}\\
\hat{x}_{\mathrm{CTL}} &= 0, && \text{(5d)}
\end{aligned}$$

where $\hat{x}_{\mathrm{T}}$, $\hat{x}_{\mathrm{MDSC}}$, $\hat{x}_{\mathrm{NK}}$, and $\hat{x}_{\mathrm{CTL}}$ represent the steady state values of x_{T}, x_{MDSC}, x_{NK}, and x_{CTL}, respectively. We observe baseline populations of MDSCs and NK cells at the metastatic site, but

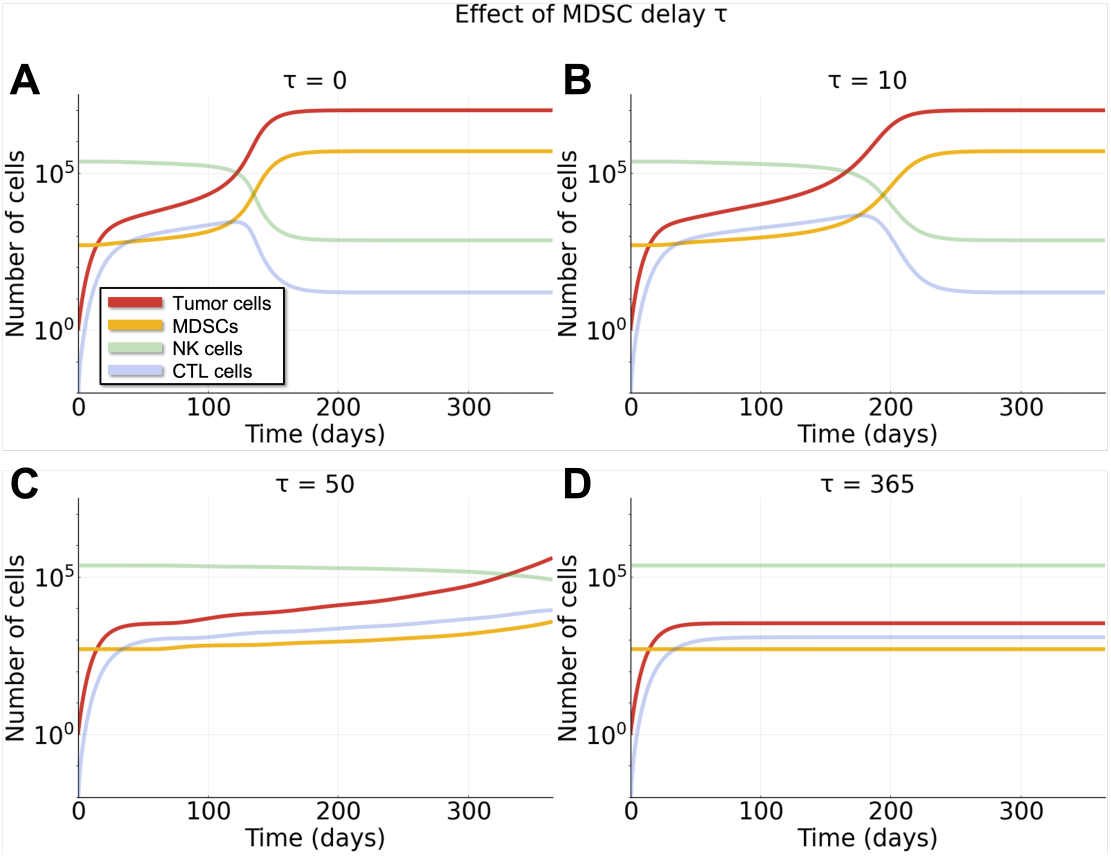

Figure 2: **Larger MDSC delays result in significantly altered tumor growth dynamics.** Simulations of the deterministic (DDE) system (Eqns. (3a)-(3d), $g = 0$) over one year, with one initial tumor cell and different MDSC delay parameter τ. See Methods for simulation details. **A**: $\tau = 0$. **B**: $\tau = 10$. **C**: $\tau = 50$. **D**: $\tau = 365$.

no CTL cells, as they need to be recruited and activated against the tumor. Since tumor cells cannot be spontaneously generated in this model, the tumor-free fixed point (Eqns. (5a)-(5d)) is stable. In the case of a nonzero tumor population ($\hat{x}_{\mathrm{T}} > 0$), in general the steady state must be determined numerically, although we can derive analytical approximations in special cases. For example, for $\hat{x}_{\mathrm{T}} > 0$, the steady states of the non-tumor populations are:

$$\hat{x}_{\mathrm{MDSC}} = \frac{\alpha_2(\hat{x}_{\mathrm{T}} + \gamma_1) + \alpha_3 \hat{x}_{\mathrm{T}}}{\zeta_2(\hat{x}_{\mathrm{T}} + \gamma_1)}, \tag{6a}$$

$$\hat{x}_{\mathrm{NK}} = \frac{\zeta_2(\hat{x}_{\mathrm{T}} + \gamma_1)\left(\alpha_4\left(\hat{x}_{\mathrm{T}}^2 + \gamma_2\right) + \alpha_5 \hat{x}_{\mathrm{T}}^2\right)}{\left(\hat{x}_{\mathrm{T}}^2 + \gamma_2\right)\left(\alpha_2\beta_3(\hat{x}_{\mathrm{T}} + \gamma_1) + \alpha_3\beta_3\hat{x}_{\mathrm{T}} + \zeta_2\zeta_3(\hat{x}_{\mathrm{T}} + \gamma_1)\right)}, \tag{6b}$$

$$\hat{x}_{\mathrm{CTL}} = \frac{\zeta_2 \hat{x}_{\mathrm{T}}(\gamma_1 + \hat{x}_{\mathrm{T}})h_1}{\left(\gamma_2 + \hat{x}_{\mathrm{T}}^2\right)\left(\gamma_3 + \hat{x}_{\mathrm{T}}^2\right)h_2}, \tag{6c}$$

where

$$\begin{aligned} h_1 &= \big(\hat{x}_{\mathrm{T}}\big(\alpha_2\beta_3\alpha_7(\gamma_1 + \hat{x}_{\mathrm{T}})\left(\gamma_2 + \hat{x}_{\mathrm{T}}^2\right) + \zeta_2\alpha_5\alpha_6\hat{x}_{\mathrm{T}}(\gamma_1 + \hat{x}_{\mathrm{T}})\left(\gamma_3 + \hat{x}_{\mathrm{T}}^2\right) + \alpha_3\beta_3\alpha_7\hat{x}_{\mathrm{T}}\left(\gamma_2 + \hat{x}_{\mathrm{T}}^2\right) \\ &+ \zeta_2\zeta_3\alpha_7(\gamma_1 + \hat{x}_{\mathrm{T}})\left(\gamma_2 + \hat{x}_{\mathrm{T}}^2\right)\big) + \zeta_2\alpha_4\alpha_6(\gamma_1 + \hat{x}_{\mathrm{T}})\left(\gamma_2 + \hat{x}_{\mathrm{T}}^2\right)\left(\gamma_3 + \hat{x}_{\mathrm{T}}^2\right)\big), \\ h_2 &= (\alpha_2\beta_3(\gamma_1 + \hat{x}_{\mathrm{T}}) + \alpha_3\beta_3\hat{x}_{\mathrm{T}} + \zeta_2\zeta_3(\gamma_1 + \hat{x}_{\mathrm{T}}))(\alpha_2\beta_4(\gamma_1 + \hat{x}_{\mathrm{T}}) + \alpha_3\beta_4\hat{x}_{\mathrm{T}} + \zeta_2\zeta_4(\gamma_1 + \hat{x}_{\mathrm{T}})). \end{aligned}$$

If we assume that the tumor reaches its carrying capacity, η, then the tumor steady state is given by Eqns. (6a)-(6c) with $\hat{x}_{\mathrm{T}} = \eta$.

We can also determine whether a small initial number of tumor cells will grow to a significantly sized positive steady state (e.g. a steady state in which $x_{\mathrm{T}} > 10$) or will initially decay. This is an important question, as we expect metastases to be seeded from a small initial number of circulating tumor cells (1, 13, 34, 37, 78). If we begin at the tumor-free steady state (Eqns. (5b)-(5d)), and increase the number of tumor cells by one or two, then taking the highest order terms in Eqn. (3a) we see that the rate of change of the tumor population will be initially positive if $\mathcal{G} > 0$. Here $\mathcal{G}$ can be defined as the tumor growth threshold, or equivalently, the tumor basic reproductive ratio (analogous to $\mathcal{R}_0$ in epidemiological models; see Supplementary Information Section S4 for details). $\mathcal{G}$ is given by:

$$\mathcal{G} = \alpha_1 \log(\eta) - \frac{\zeta_2\beta_1\alpha_4}{\alpha_2\beta_3 + \zeta_2\zeta_3} - \zeta_1. \tag{7}$$

Examples of simulations starting from the tumor-free steady state (Eqns. (5b)-(5d)) but with the addition of a single tumor cell are shown in Figure 3A-C. The tumor population grows initially if and only if $\mathcal{G} > 0$. In Figure 3A the parameter values are as defined in Table 1, giving $\mathcal{G} \approx 0.8$, and a resulting tumor size at steady state of 9.8×10^6. We change the tumor cell death rate (ζ_1) to vary $\mathcal{G}$: to $\mathcal{G} \approx 0$ (giving a tumor steady state of ≈ 1; Figure 3B), and to $\mathcal{G} \approx -0.2$ (giving a tumor steady state of < 1; Figure 3C). The threshold $\mathcal{G}$ thus gives an approximation of whether small numbers of tumor cells will grow into fully developed metastases, of relevance for cancer prognosis, treatment, and progression (36).

3.2 Parameter sensitivity analysis reveals that inhibition rates between populations are most important in determining tumor growth outcomes

We perform parameter sensitivity analysis to assess the relative importance of model parameters on the growth and final size of the tumor population. Since the tumor steady state is independent of the MDSC delay as $t \to \infty$, for sensitivity analysis we set the delay $\tau = 0$.

As seen in the model (Eqns. (3a)-(3d)), the MDSC-specific parameters are α_2, α_3, ζ_2, β_3, β_4, and γ_1. The Morris global sensitivity analysis for the effect of the MDSC-specific parameters on the tumor population steady state (numerically calculated) is shown in Figure 3D, where the MDSC-specific parameters are marked by large hexagons. The green (red) color denotes parameters that

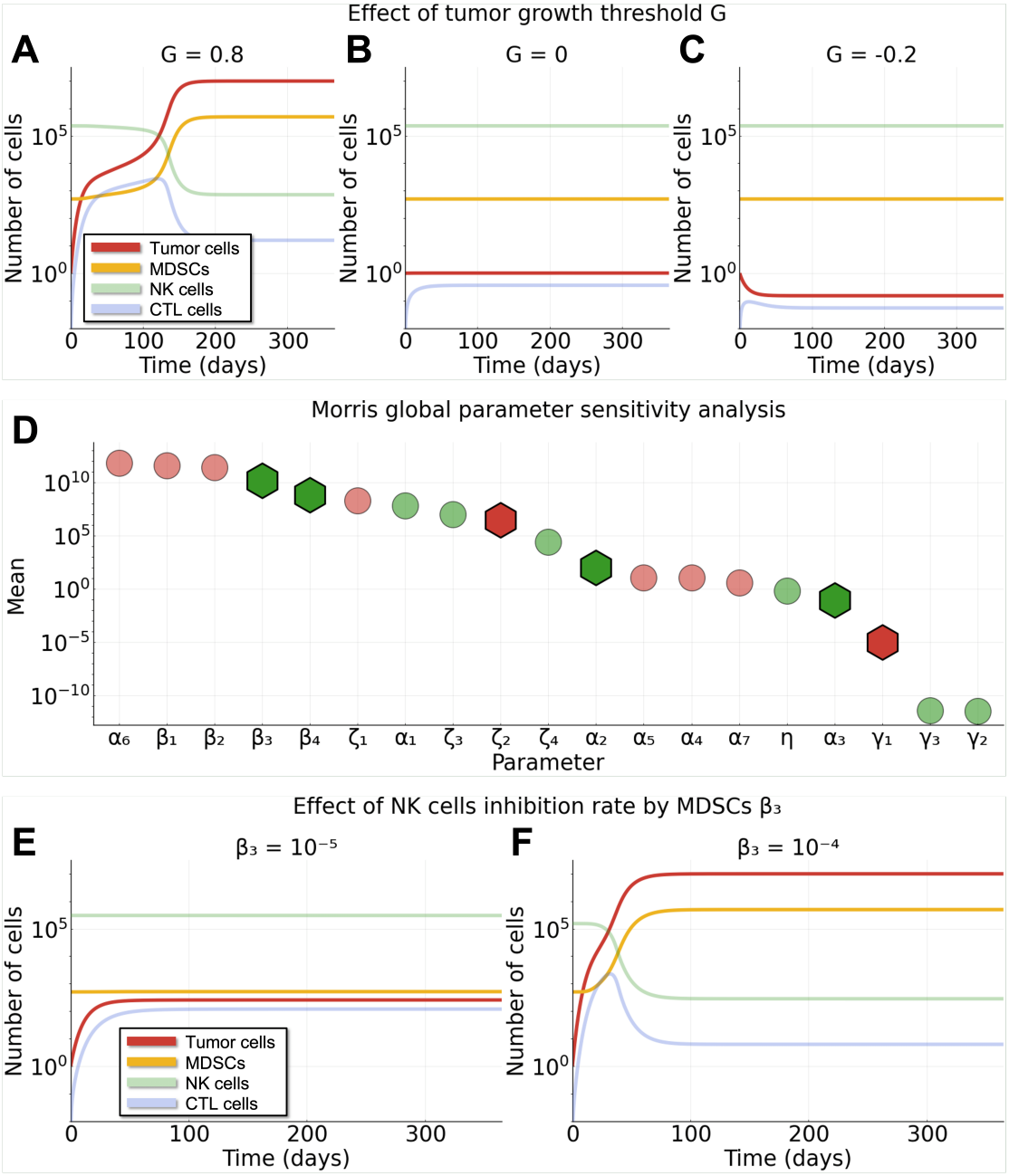

Figure 3: **Dependencies of tumor growth characteristics on model parameters.** Simulations of the ODE system (Eqns. (3a)-(3d), $g = \tau = 0$) with one initial tumor cell. **A-C**: Different tumor growth thresholds $\mathcal{G}$ (Eqn. (7)). (A); $\mathcal{G} \approx 0.8$ (parameters as in Table 1). (B); $\mathcal{G} \approx 0$ ($\zeta_1 = 0.81$). (C); $\mathcal{G} \approx -0.2$ ($\zeta_1 = 1$). **D**: Morris global sensitivity analysis (GSA) for the steady state of the tumor population for all model parameters. Green denotes parameters that are positively correlated with the tumor size at steady state; red denotes negatively correlated. Hexagons represent MDSC-specific parameters; circles represent non-MDSC-specific parameters. **E-F**: Effects of the NK inhibition rate by MDSCs (β_3), for $\beta_3 = 10^{-5}$, the minimum of the GSA range (E); the tumor size at steady state is 2.5×10^2. And for $\beta_3 = 10^{-4}$, the maximum of the GSA range (F); The tumor size at steady state is 9.9×10^6.

are positively (negatively) correlated with the steady state of the tumor population. As expected, ζ_2 (death rate of MDSCs) and γ_1 (steepness of MDSC production) are the only MDSC-specific parameters negatively correlated with the tumor population, as increasing either of these parameters results in fewer MDSCs and thus a more immunosusceptible tumor population.

In Figure 3D we also see that β_3 (inhibition of NK cells by MDSCs) is the most important MDSC-specific parameter for the tumor steady state. This is because initially the NK cell population is very large (77) (see the green line in Figure 2 and Eqn. (5c)) and the MDSC population must effectively suppress the NK cells for the tumor to be able to grow and not die out quickly. Similarly, β_4 (inhibition of CTL cells by MDSCs) is also very important, but less so than β_3 as the CTL population is initially small and so less important to the initial growth of the tumor (see the blue line in Figure 2 and Eqn. (5d), and the Discussion for consideration of CTL rich environments).

Figure 3E-F explicitly shows the effect of β_3 (inhibition of NK cells by MDSCs) on the tumor steady state at both ends of the GSA range. Here, we see that small β_3 (Figure 3E) results in a small metastatic tumor ($\beta_3 = 10^{-5}$, tumor population steady state 2.5×10^2) whereas large β_3 (Figure 3F) results in a large metastatic tumor ($\beta_3 = 10^{-4}$, tumor population steady state 9.9×10^6).

The Morris global sensitivity analysis for all model parameters is shown in Figure 3D, (non-MDSC parameters marked by circles) where again the green (red) color denotes parameters that are positively (negatively) correlated with the steady state of the tumor population. Here we see that α_2, α_3, α_1, η, β_3, ζ_3, β_4, ζ_4, γ_2, and γ_3 are positively correlated with the tumor population steady state and all other parameters are negatively correlated. The most important parameters (as measured by their effect on the tumor steady state) are α_6, β_1, β_2, β_3 and β_4, where α_6 is the rate of CTL stimulation by tumor-NK cell interaction, β_1 and β_2 are inhibition rates of tumor cells by NK and CTL cells, and β_3 and β_4 are inhibition rates of NK and CTL cells by MDSCs (see Table 1 for a full list of parameter descriptions). Therefore, our model dynamics are largely influenced by inhibition/stimulation between competing populations (see Figure 1 for schematic diagram), which makes sense as these interactions (especially recently in the context of increased focus on MDSC populations) have been shown to be important determinants of cancer dynamics in tumor microenvironments (1, 8, 10, 17, 20, 21, 42).

3.3 Stochastic dynamics of metastatic growth and establishment

We now turn to analysis of the stochastic dynamics of the model. Given the seeding of metastases by one or a few cells, stochastic effects are likely to play a large role in the system. In order to study metastatic tumor establishment and viability we simulate the SDDE model (Eqns. (3a)-(3d)), with MDSC delay $\tau \geq 0$.

Stochastic simulations allow for the probabilistic analysis of "successful metastases". In the deterministic setting, $\mathcal{G}$ determines whether a new metastasis forms: using the parameters defined in Table 1, a metastatic tumor is always formed ($\mathcal{G} > 0$). In the stochastic setting, this is no longer the case. Model outcomes vary even for identical initial conditions due to the noise in the system (10, 79, 80). Although we do not study the sources of biological noise here, we expect the major component to result from noise in the intercellular signaling processes, i.e. extrinsic noise (81).

To study the probability that a small number of pioneering cells will establish a new metastasis, we start simulations with (the continuous differential equation equivalent of) two tumor cells, and denote a metastasis successful if the number of tumor cells does not drop below one (i.e. $\lfloor x_T(t) \rfloor > 0$) in a one-year timespan ($t \in [0, 365]$ days). Figure 4 shows examples of both successful metastatic tumors (panels A and C) and unsuccessful metastatic tumors (panels B and D) for different values of the MDSC delay τ (see Supplementary Information Section S3 for further description). For more examples of successful and unsuccessful tumors see Figures S2 and S3 respectively. While a metastatic tumor can become unsuccessful at any time point (and all tumors will be unsuccessful almost surely as $t \to \infty$), the tumor population is most likely to drop below one near the beginning

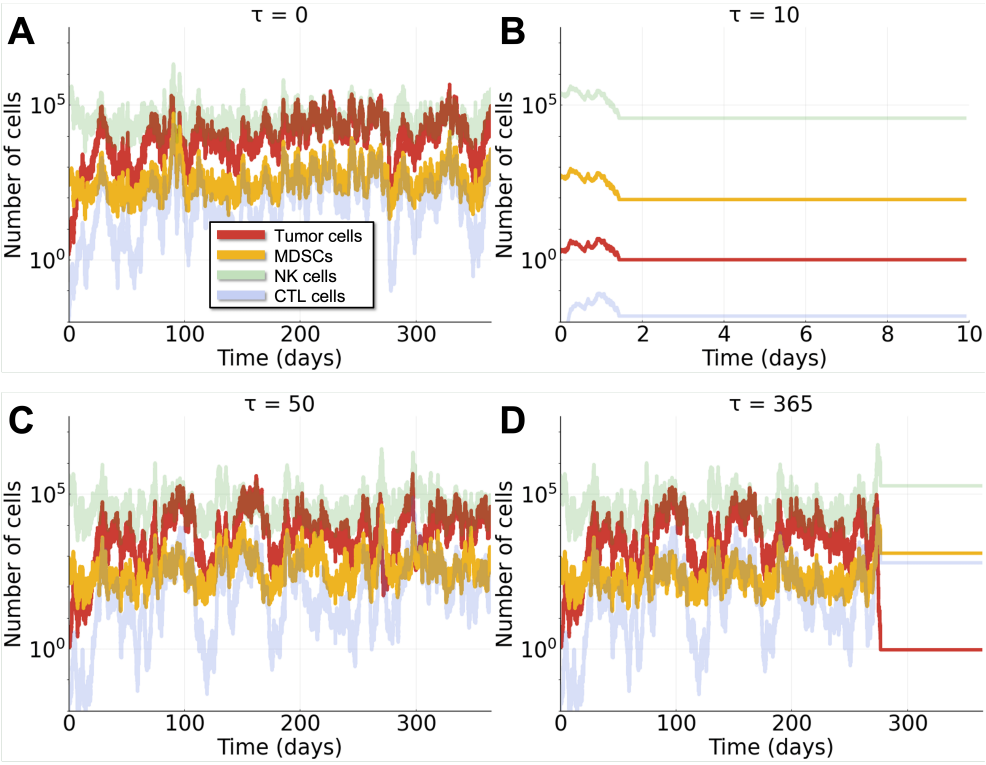

Figure 4: **Stochastic effects influence the growth and probability of establishment of metastatic tumors.** Examples of simulations of the SDDE system (Eqns. (3a)-(3d)) over one year, with two initial tumor cells and different values of the MDSC delay parameter, τ. A "successful" metastatic tumor is one that does not drop below a size of one tumor cell over the simulation period. **A**: $\tau = 0$; successful. **B**: $\tau = 10$; unsuccessful. **C**: $\tau = 50$; successful. **D**: $\tau = 365$; unsuccessful.

of the simulation (i.e. soon after metastatic tumor seeding) when the tumor population is small (Figures S4 and S5).

3.4 Delays in MDSC recruitment decrease the probability of metastasis and the size of metastatic tumors

Analysis of the probability of metastasis under different assumptions of MDSC-tumor-immune interactions for thousands of tumors studied *in silico* revealed striking dependencies of tumor outcomes on MDSC dynamics (Figure 5). Through joint analysis of the effects of the number of circulating MDSCs (α_2) and the size of the MDSC delay (τ), we found that the probability of successful metastatic tumor establishment and the average size of metastatic tumors are positively correlated with the level of circulating MDSCs, and negatively correlated with the size of the MDSC delay. As more MDSCs become available at or near the site of the nascent metastasis, the NK and CTL populations become more suppressed, resulting in a greater likelihood of tumor growth (Figure 5A-B). Importantly: the positive feedback loop (tumor cells are able to activate more MDSCs) reinforces the tumor's ability to grow even in a "hot" tumor.

We found that our model provides novel and biologically-driven means to determine exactly what can be inferred from levels of circulating MDSCs. Given the relative difficulty of defining MDSCs and the relative ease of sampling circulating cells this bears important clinical relevance (19). If the baseline level of circulating MDSCs (α_2) is high, MDSC activation delays have little effect on the metastasis establishment probability (Figure 5A-B), but the MDSC delay still has a pronounced effect on the resulting sizes of the metastases that grow (Figure 5C-D and Figure S6).

Recall that our definition of successful metastasis is liberal: a population of > 1 tumor cells that survives for a year. Differences in the sizes of these nascent metastases from tens to thousands of cells bear direct clinical relevance. Further statistics on metastatic survival and size can be found in Table S1. Relative to a MDSC delay of 0 days, a MDSC delay of 365 days leads to a 2-fold decrease in the probability of successful metastasis, a 21-fold decrease in the mean tumor size (of successful tumors), and a 4.6-fold increase in the mean time to extinction of unsuccessful metastases.

Figure S7 shows the effect of the rate of MDSC inhibition of NK cells (β_3) and Figure S8 shows the effect of the rate of MDSC inhibition of CTL cells (β_4). Here, we see that more effective (i.e. more inhibitory against anti-tumor populations) MDSCs ($\beta_3, \beta_4 \uparrow,\ \tau \downarrow$) means NK and CTL populations are more inhibited, which results in more tumor cells. However, if the level of inhibition of NK cells (β_3) is high enough, delays in recruitment of more MDSCs (τ) has little effect on the probability of successful metastatic tumors (as the tumor population will grow to very large levels very quickly, independently of a large increase in the number of MDSCs) but still effects the average size as less NK cells results in more tumor cells (Figure S7). Since there are initially zero CTL cells and the CTL population does not reach extremely high levels relative to other populations (see for instance Figure 2, blue lines) changing β_4 does not have a large effect on the probability of successful metastasis (Figure S8A-B). However, increasing β_4 can result in a small increase in the average size of successful tumors (see Figure S8C-D).

MDSCs can be sub-divided into one of two states: monocytic M-MDSCs (typically assumed to be more immunosuppressive) and granulocytic/poly-mononuclear (G- or PMN-MDSCs) (1, 3, 6). The relative proportion of G- to M-MDSCs can alter the immunosuppressive properties of the tumor microenvironment (15, 82). For example, if the relative proportion of G- to M-MDSCs skews toward M-MDSCs, we would expect larger effects of MDSC delays (as seen in Figure 5), whereas the opposite would be expected if G-MDSCs dominate. Extensions of the current model include separating M-MDSCs and G-MDSCs, with for instance $\beta_3^{\text{M-MDSCs}} > \beta_3^{\text{G-MDSCs}}$ and $\beta_4^{\text{M-MDSCs}} > \beta_4^{\text{G-MDSCs}}$, see the Discussion for further details.

To summarize the results of this section, we have identified two crucial effects of MDSC delays on the stochastic tumor dynamics. First, that MDSC delays always result in significantly smaller tumor sizes. This effect is pronounced when MDSCs are more immune-suppressive (i.e. when β_3, β_4 are large). Under these conditions, the increase in MDSCs most allows the tumor to outcompete the anti-tumor populations and reach large sizes. However if the MDSCs are so powerful as to completely inhibit the NK and CTL populations, then increasing β_3, β_4 will have no further effect. The effect of MDSC delay on tumor size is less pronounced when the MDSCs are less immune-suppressive (i.e. when β_3, β_4 are small): in this case increases in the number of MDSCs will not have significant effects on the long term dynamics of the other populations.

Second, that MDSC delays can result in drastically decreased probabilities of a successful new metastasis. This effect is most pronounced when the initial level of circulating MDSCs (α_2) is not too high, and when the MDSCs are not too immune-suppressive of the NK population (large β_3). This is due to the greater likelihood of extinction of stochastic tumors ($\lfloor x_{\text{T}} \rfloor < 1$) early in the simulation. If the level of circulating MDSCs (α_2) is high, offering the nascent tumor protection against CTL and NK cell responses, then the effects of delays in recruitment of more MDSCs are lessened. Similarly, if the MDSCs are strongly immune-suppressive (particularly against NK cells), then the tumor is likely to grow to a large size quickly, negating the impact of delays in MDSC recruitment on the probability of successful establishment of a new metastasis. These results establish how MDSC plasticity, as defined by their different suppressive functions and environments (i.e. circulation throughout the body or within a tumor), differentially contribute to tumor growth and progression of disease from a primary tumor location to a distant metastatic site.

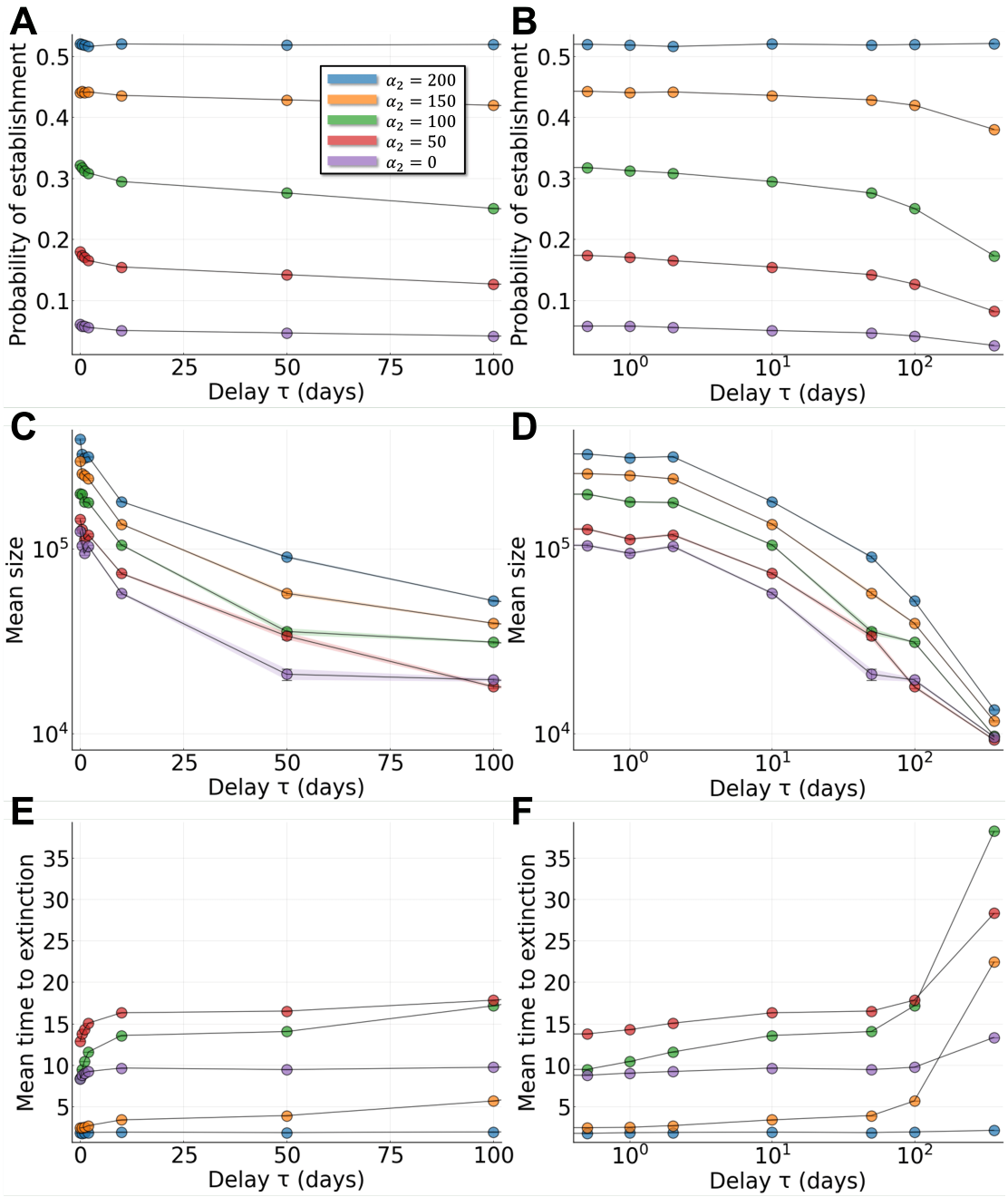

Figure 5: **Effects of MDSC properties on the probability of metastatic establishment.** Stochastic simulations run for a period of one year. Each point is the mean over at least 10^5 simulations. Ribbons (shaded area) represent the standard error. **A**: Probability of new tumor establishment over a period of one year, for different values of the level of circulating MDSCs (α_2) and the MDSC delay (τ). **B**: As for A with τ plotted on log scale. **C**: Of the new metastases that are successfully established, the distribution of their means sizes is given. **D**: As for C with τ plotted on log scale. **E**: Of the new metastases that go extinct, the distribution of the mean times to extinction is given. **F**: As for E with τ plotted on log scale.

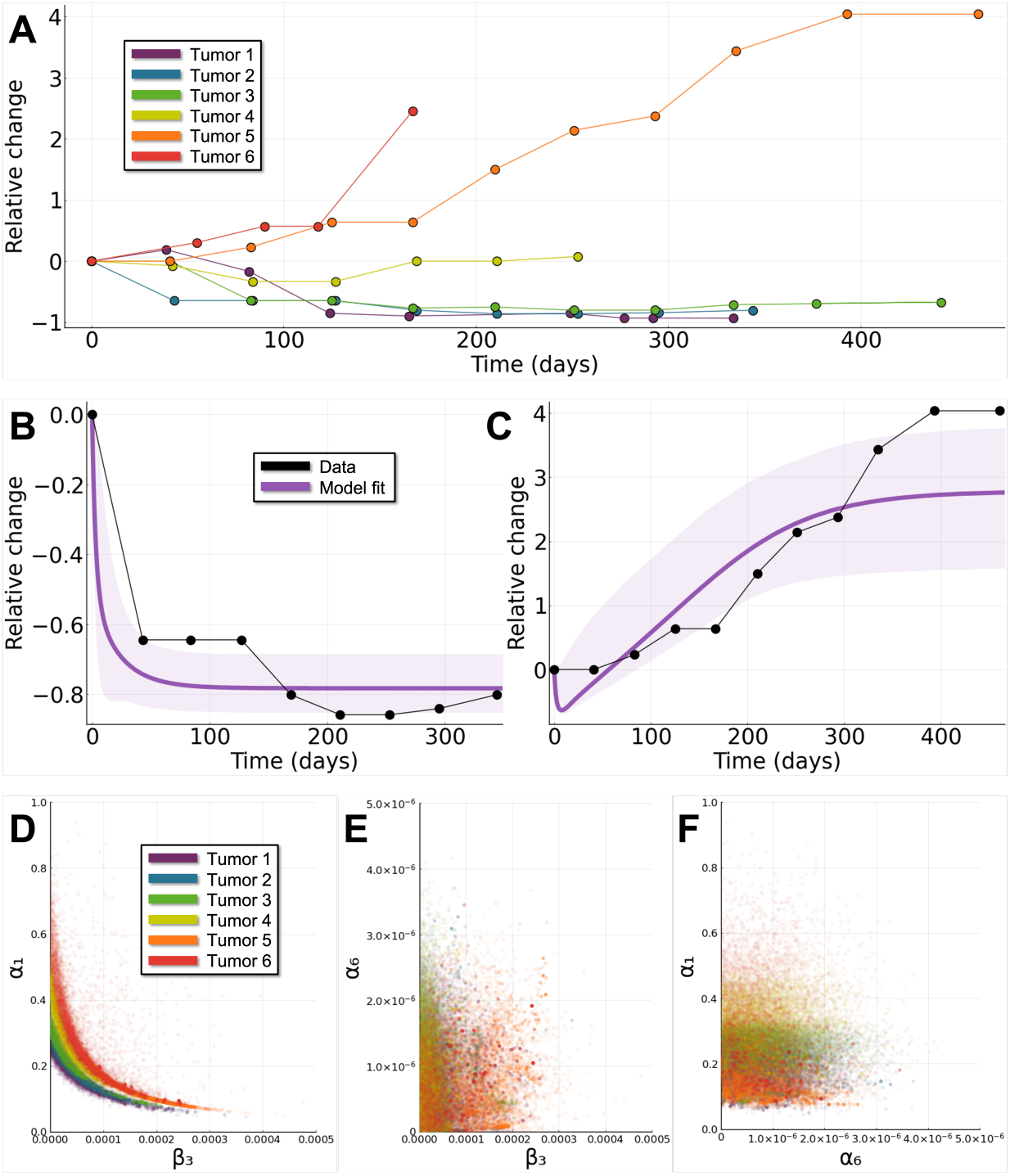

Figure 6: **Interactions between MDSCs and NK cells control clinical tumor growth outcomes.** **A**: Relative change in tumor size from the baseline assessment for six tumors from non-small cell lung cancer patients undergoing treatment with anti-PD-L1. Tumors are ordered (1-6) by their response, compared to baseline assessment. **B**: Tumor 2 model trajectories based on the relative change in the tumor population with the black dots representing the data, the purple line representing the fit from using the median of the posterior distribution for each parameter, and the shaded area denoting the 90% credible interval (where 90% of the posterior trajectories lie). **C**: Same as B for tumor 5. **D-F**: Samples from the posterior distribution of each of the six tumors, 8×10^3 samples plotted for pairs of model parameters: (D); NK cell inhibition rate by MDSCs (β_3) versus tumor growth rate (α_1). (E); NK cell inhibition rate by MDSCs (β_3) versus CTL stimulation by tumor-NK cell interaction (α_6) (F); CTL stimulation by tumor-NK cell interaction (α_6) versus tumor growth rate (α_1).

3.5 Bayesian parameter inference reveals the importance of MDSC-NK cell interactions in determining clinical outcomes

In order to assess more rigorously the variability and uncertainty with which we know model parameters, we performed Bayesian parameter inference using clinical data on tumor progression as defined through RECIST ((38) and see Methods). We fit our tumor-immune model to data from six individual tumors that broadly span the possible *in vivo* response outcomes (Figure 6A). We selected a three-dimensional parameter space to study important parameters as identified previously, consisting of the tumor growth rate, the NK inhibition rate by MDSCs, and the rate of CTL stimulation by tumor-NK cell interactions. Successful fits were obtained for each of the tumors fit (Figure 6B-C and Supplementary Information Section S5).

To analyze the parameters that give rise to different response dynamics, we plot parameters sampled from the posteriors of each tumor fit (Figure 6D-F). We can see a clear trend towards larger values of tumor growth rate (α_1) and NK inhibition rate by MDSCs (β_3) for tumors that do not respond to treatment (tumors 5 & 6) compared to those that do respond to treatment (tumors 1 & 2) (Figure 6D). This can be understood in light of the previously characterized effects these parameters have on tumor growth (see e.g. Figure 3D). Furthermore, strong correlations can be observed for these parameters. The correlation between the two parameters is steeper for increasing tumors, suggestive of the discriminative ability of this parameter pair for quantifying tumor outcomes (i.e. whether tumors will grow or decay upon the initiation of treatment). In comparison, no correlations nor distinct effects on tumor outcomes are observed for the other two parameter pairs (Figure 6E-F).

We tested the discriminative power of different combinations of posterior parameters by training decision trees to classify tumor responses as either decreasing (i.e. tumors 1 & 2) or increasing (i.e. tumors 5 & 6) over time. Table 2 gives the cross validation scores for decision trees (maximum depth three) trained on different sets of posterior parameters as features. In line with the marginal posteriors (Figure 6D) we see that the best discriminative power is obtained using both the tumor growth rate (α_1) and the NK cell inhibition rate by MDSCs (β_3) as features. Strikingly, constrained to using one feature, the NK cell inhibition rate by MDSCs is a better predictor than the tumor growth rate, even though the tumor growth rate is intricately tied to the classification outcome (43). Interest in interactions between MDSCs and NK cells has already been growing in recent years (20, 21, 24); this result urges that much more investigation is warranted.

Given that the clinical data available for inference do not capture immune dynamics, coupled with the relative simplicity of the tumor dynamics in response to treatment, we expected to be able to obtain fits to various individual tumor outcomes with our tumor-immune model. However, the relative importances of parameters that this data fitting revealed were completely unexpected. The strength of immune-suppressiveness – as controlled by NK cell inhibition by MDSCs – was identified as the most important parameter in determining outcome. This has direct clinical implications: while it may not yet be possible to directly modulate this parameter in a clinical setting, it highlights the importance of interventions targeting properties of MDSCs in and around the tumor site. Moreover, successfully fitting of various tumor responses to tumor-MDSC dynamics and the stratification of rate parameters that resulted demonstrates our ability to build and fit patient-specific tumor growth models (83), with which to predict metastatic outcomes.

4 Discussion

Cancer dynamics are complex, and understanding cancer-immune dynamics is a complex systems biology problem (10, 28, 29, 39, 43). Modeling how tumors interact with the immune system is critical for understanding treatment responses and predicting the best possible therapeutic strategies in response to metastasis. Myeloid-derived suppressor cells (MDSCs) have been identified in various tumor microenvironments (8, 9, 15), where they can exert strong immunosuppressive effects leading

Features for prediction	Three-fold cross validation scores
α_1	62.8 ± 5.68
β_3	69.1 ± 5.12
α_6	55.6 ± 4.51
(α_1, β_3)	81.5 ± 7.88
(α_1, α_6)	63.0 ± 5.37
(β_3, α_6)	68.2 ± 5.60
$(\alpha_1, \beta_3, \alpha_6)$	81.5 ± 7.88

Table 2: **Classification of tumor responses using posterior parameters shows relationship between tumor growth and MDSC inhibition rates.** Decision trees were used to classify tumor responses as either decreasing (tumors 1 & 2) or increasing (tumors 5 & 6) based on sets of one or two posterior parameters as features. Three-fold cross validation scores are given as mean ± standard deviation.

to worse outcomes (12, 17, 37), yet a rigorous theoretical characterization of MDSC dynamics in the tumor microenvironment has remained lacking. Here, through the introduction of a stochastic delay differential equation (SDDE) model with which to study tumor-MDSC dynamics, we have provided means to characterize the plasticity of MDSCs and their effects on tumor progression and outcome.

With this model we began by studying outcomes under simple, idealized circumstances, such as: how large do tumors grow in the presence of MDSCs? What is their likelihood of persistence in the stochastic case? We discovered that delays in MDSC recruitment/activation have striking effects on metastatic growth and establishment. Under certain conditions (lower levels of circulating MDSCs), strategies that block MDSC recruitment to the site of the tumor are likely to greatly improve metastatic outcomes and hinder growth. We also demonstrated through model analyses how strategies that decrease the immunosuppressive properties of MDSCs can have dramatic anti-tumor effects. Via Bayesian parameter estimation using data from tumor growth *in vivo*, we have found interesting and novel correlations between the tumor and the MDSC response parameters, again demonstrating the potential of inhibition of MDSCs as a desirable drug target.

Our inference results showed that the MDSC inhibition of NK cells was a crucial parameter informing outcomes; more important than the tumor growth rate, as well as the MDSC inhibition of CTL cells. It is important to note that there will be differences between tumor microenvironments: here we studied MDSC dynamics in the lungs, an NK cell rich environment (24, 77). If we were to study MDSC dynamics in different environments, such as those in which CTL cells are greater in number than NK cells, we would likely observe different model effects dominating, e.g. the role of CTL activation might rise in prominence (84–88).

These results suggest that the identification of effective anti-MDSC treatment strategies to control cancer growth and spread ought to be more highly prioritized (8, 13, 17, 24). In particular, drug treatments that block MDSC recruitment to tumor sites and/or target MDSCs in the lymphoid organs seem to be most highly effective in preventing metastasis, but their effects are lessened if the level of circulating MDSCs is low, or if MDSCs are less effective at suppressing anti-tumor populations. Since the level of circulating MDSCs (as well as the level of MDSC-immunosuppresion) is likely to be highly variable within patients (20, 59), effective treatment strategies ought to be informed by patient-specific biomarkers (83, 89). In addition, evaluation of the phentoype of circulating MDSCs may not fully reflect the immunosuppressed state within tumors enough to predict potential response to immunotherapy, which may be determined in part by further mathematical and data-driven modeling. Towards this end, we have shown via tumor-specific parameter inference that we can train machine learning models using posterior parameters to classify metastatic outcomes. Future work, informed by more data (such as richer dynamic information or single-cell gene expression data) will provide additional means to classify treatment outcomes. In this context

it will be important to consider the prediction of responses in different tumor microenvironments and under different treatment regimes.

MDSCs cannot be assumed to be a homogeneous population. Although we have assumed as such here – for lack of data with which to quantify subpopulation-specific MDSC rate parameters – future models ought to consider MDSC heterogeneity. MDSCs are typically classified into one of two possible cell types, monocytic (M-MDSCs) and granulocytic/polymononuclear (G-/PMN-MDSCs), which exhibit different levels of immunosuppression (1, 3, 15). M-MDSCs in metastatic breast cancer patients resemble monocytes isolated from patients with sepsis, indicating fascinating similarities between the immunosuppression capability of the MDSCs present in metastatic (but perhaps not primary) breast cancer patients and those involved in the immunosuppressive sepsis response (90). Further measurement of MDSC subtype-specific immunosuppression *in vivo* will likely yield substantial new insight into their activity. Moreover, these additional data will permit the fitting of more detailed mathematical models that are able to describe patient-specific (or even tumor site-specific) dynamics, and quantify the possible benefits of treatments targeting MDSCs. Current knowledge suggests that shifting MDSC phenotypes towards G-MDSCs is beneficial as this state is less immunosuppresive (1, 15), however further characterization of these states is needed.

The models we have developed of MDSCs in the tumor microenvironment do not consider space, although of course spatial architectures play an important role in tumor progression (28, 32), in primary growth as well as for circulating tumor cells that seed metastases (34, 91). The role of spatial aspects of cancer niches in regulating MDSC-tumor dynamics will be an important topic in future work (92). Here, carefully fitting models to appropriate data ought to include both single-cell-resolved characterization of the tumor microenvironment (15) and explicit spatial characterizations (93, 94).

There is an urgent need to understand the role of MDSC dynamics during tumor growth and metastasis. Here we discovered an essential and remarkable role for MDSC recruitment/activation in dictating growth outcomes in the context of new metastases. This is but the first step. To make progress further conceptual model development tightly linked to inference and the gathering of higher-resolution data on MDSC phenotypes *in vivo* will be crucial. Mathematical modeling will continue to play an integral part in discovery as it allows us to account for the numerous and dynamic factors controlling MDSC plasticity and its impact of tumor responses in a way that traditional biologic biomarkers alone cannot. Only by developing theory and gathering data hand-in-hand can we hope to gain an understanding of the dynamics of MDSCs in the tumor microenvironment, and in turn, develop new therapies for metastatic disease.

Author Contributions

J.K., E.R.T., and A.L.M. conceived the project. J.K. and A.L.M. developed the model and the software. J.K., E.R.T., and A.L.M. analyzed data. J.K. and A.L.M. wrote the paper with input from all the authors.

Funding Statement

E.R.T. acknowledges support from the Tower Cancer Research Foundation (Career Development Award), the Concern Foundation (Conquer Cancer Award), and the USC-Norris Comprehensive Cancer Center. A.L.M. acknowledges support from the National Institutes of Health (R35GM143019) and the National Science Foundation (DMS2045327).

Conflict of Interest Statement

The authors declare no competing interests.

Data Availability Statement

All code and data is available at a public github repository located here: https://github.com/maclean-lab/ModelingMDSCs and tumor data (38, 69) is also available in the supplementary file tumor_data.xlsx.

Acknowledgments

We would like to thank all members of the Roussos Torres and MacLean labs for valuable input and discussions. Figure 1 was created with BioRender (BioRender.com).

References

[1] Veglia, F., Sanseviero, E. & Gabrilovich, D. I. Myeloid-derived suppressor cells in the era of increasing myeloid cell diversity. *Nature Reviews Immunology* **21**, 485–498 (2021). URL `https://www.nature.com/articles/s41577-020-00490-y`.

[2] Hegde, S., Leader, A. M. & Merad, M. MDSC: Markers, development, states, and unaddressed complexity. *Immunity* **54**, 875–884 (2021). URL `https://www.sciencedirect.com/science/article/pii/S1074761321001667`.

[3] Bergenfelz, C. & Leandersson, K. The Generation and Identity of Human Myeloid-Derived Suppressor Cells. *Frontiers in Oncology* **10** (2020). URL `https://www.frontiersin.org/article/10.3389/fonc.2020.00109`.

[4] Talmadge, J. E. & Gabrilovich, D. I. History of myeloid-derived suppressor cells (MDSCs) in the macro- and micro-environment of tumor-bearing hosts. *Nature Reviews. Cancer* **13**, 739–752 (2013).

[5] Bronte, V. *et al.* Recommendations for myeloid-derived suppressor cell nomenclature and characterization standards. *Nature Communications* **7**, 12150 (2016). URL `https://www.nature.com/articles/ncomms12150`.

[6] Veglia, F., Perego, M. & Gabrilovich, D. Myeloid-derived suppressor cells coming of age. *Nature Immunology* **19**, 108–119 (2018). URL `https://www.nature.com/articles/s41590-017-0022-x`.

[7] Alshetaiwi, H. *et al.* Defining the emergence of myeloid-derived suppressor cells in breast cancer using single-cell transcriptomics. *Science Immunology* **5** (2020). URL `https://immunology.sciencemag.org/content/5/44/eaay6017`. Publisher: Science Immunology Section: Research Resources.

[8] Tesi, R. J. MDSC; the Most Important Cell You Have Never Heard Of. *Trends in Pharmacological Sciences* **40**, 4–7 (2019). URL `https://www.sciencedirect.com/science/article/pii/S0165614718301895`.

[9] Ren, L. *et al.* Single cell RNA sequencing for breast cancer: present and future. *Cell Death Discovery* **7**, 1–11 (2021). URL `https://www.nature.com/articles/s41420-021-00485-1`.

[10] Hamilton, P. T., Anholt, B. R. & Nelson, B. H. Tumour immunotherapy: lessons from predator–prey theory. *Nature Reviews Immunology* 1–11 (2022). URL `https://www.nature.com/articles/s41577-022-00719-y`.

[11] Wynn, T. A. Myeloid-cell differentiation redefined in cancer. *Nature immunology* **14**, 197–199 (2013). URL `https://www.ncbi.nlm.nih.gov/pmc/articles/PMC3806344/`.

[12] Cha, Y. J. & Koo, J. S. Role of Tumor-Associated Myeloid Cells in Breast Cancer. *Cells* **9**, 1785 (2020). URL `https://www.ncbi.nlm.nih.gov/pmc/articles/PMC7464644/`.

[13] Kumar, V., Patel, S., Tcyganov, E. & Gabrilovich, D. I. The nature of myeloid-derived suppressor cells in the tumor microenvironment. *Trends in immunology* **37**, 208–220 (2016). URL `https://www.ncbi.nlm.nih.gov/pmc/articles/PMC4775398/`.

[14] Tcyganov, E., Mastio, J., Chen, E. & Gabrilovich, D. I. Plasticity of myeloid-derived suppressor cells in cancer. *Current Opinion in Immunology* **51**, 76–82 (2018). URL `https://www.sciencedirect.com/science/article/pii/S0952791517301097`.

[15] Sidiropoulos, D. N. *et al.* Entinostat Decreases Immune Suppression to Promote Antitumor Responses in a HER2+ Breast Tumor Microenvironment. *Cancer Immunology Research* **10**, 656–669 (2022). URL `https://doi.org/10.1158/2326-6066.CIR-21-0170`.

[16] Christmas, B. J. *et al.* Entinostat converts immune-resistant breast and pancreatic cancers into checkpoint-responsive tumors by reprogramming tumor-infiltrating MDSCs. *Cancer immunology research* **6**, 1561–1577 (2018). URL `https://www.ncbi.nlm.nih.gov/pmc/articles/PMC6279584/`.

[17] De Cicco, P., Ercolano, G. & Ianaro, A. The New Era of Cancer Immunotherapy: Targeting Myeloid-Derived Suppressor Cells to Overcome Immune Evasion. *Frontiers in Immunology* **11**, 1680 (2020).

[18] Gonda, K. *et al.* Myeloid-derived suppressor cells are increased and correlated with type 2 immune responses, malnutrition, inflammation, and poor prognosis in patients with breast cancer. *Oncology Letters* **14**, 1766–1774 (2017).

[19] Angell, T. E. *et al.* Circulating Myeloid-Derived Suppressor Cells Predict Differentiated Thyroid Cancer Diagnosis and Extent. *Thyroid: Official Journal of the American Thyroid Association* **26**, 381–389 (2016).

[20] Tumino, N. *et al.* Interaction Between MDSC and NK Cells in Solid and Hematological Malignancies: Impact on HSCT. *Frontiers in Immunology* **12**, 316 (2021). URL `https://www.frontiersin.org/article/10.3389/fimmu.2021.638841`.

[21] Bruno, A., Mortara, L., Baci, D., Noonan, D. M. & Albini, A. Myeloid Derived Suppressor Cells Interactions With Natural Killer Cells and Pro-angiogenic Activities: Roles in Tumor Progression. *Frontiers in Immunology* **10**, 771 (2019). URL `https://www.ncbi.nlm.nih.gov/pmc/articles/PMC6482162/`.

[22] Hoechst, B. *et al.* Myeloid Derived Suppressor Cells Inhibit Natural Killer Cells in Patients with Hepatocellular Carcinoma via the NKp30 Receptor. *Hepatology (Baltimore, Md.)* **50**, 799–807 (2009). URL `https://www.ncbi.nlm.nih.gov/pmc/articles/PMC6357774/`.

[23] Cao, Y., Feng, Y., Zhang, Y., Zhu, X. & Jin, F. L-Arginine supplementation inhibits the growth of breast cancer by enhancing innate and adaptive immune responses mediated by suppression of MDSCs in vivo. *BMC cancer* **16**, 343 (2016).

[24] Zalfa, C. & Paust, S. Natural Killer Cell Interactions With Myeloid Derived Suppressor Cells in the Tumor Microenvironment and Implications for Cancer Immunotherapy. *Frontiers in Immunology* **12** (2021). URL https://www.frontiersin.org/article/10.3389/fimmu.2021.633205.

[25] Markowitz, J., Wesolowski, R., Papenfuss, T., Brooks, T. R. & Carson, W. E. Myeloid-derived suppressor cells in breast cancer. *Breast Cancer Research and Treatment* **140**, 13–21 (2013). URL https://doi.org/10.1007/s10549-013-2618-7.

[26] Jarrett, A. M. *et al.* Experimentally-driven mathematical modeling to improve combination targeted and cytotoxic therapy for HER2+ breast cancer. *Scientific Reports* **9**, 12830 (2019). URL https://www.nature.com/articles/s41598-019-49073-5.

[27] Lai, X. *et al.* Modeling combination therapy for breast cancer with BET and immune checkpoint inhibitors. *Proceedings of the National Academy of Sciences of the United States of America* **115**, 5534–5539 (2018).

[28] Mahlbacher, G. E., Reihmer, K. C. & Frieboes, H. B. Mathematical modeling of tumor-immune cell interactions. *Journal of Theoretical Biology* **469**, 47–60 (2019). URL https://www.sciencedirect.com/science/article/pii/S0022519319300955.

[29] Louzoun, Y. The evolution of mathematical immunology. *Immunological Reviews* **216**, 9–20 (2007). URL https://onlinelibrary.wiley.com/doi/abs/10.1111/j.1600-065X.2006.00495.x.

[30] Shariatpanahi, S. P., Shariatpanahi, S. P., Madjidzadeh, K., Hassan, M. & Abedi-Valugerdi, M. Mathematical modeling of tumor-induced immunosuppression by myeloid-derived suppressor cells: Implications for therapeutic targeting strategies. *Journal of Theoretical Biology* **442**, 1–10 (2018).

[31] Allahverdy, A. *et al.* An agent-based model for investigating the effect of myeloid-derived suppressor cells and its depletion on tumor immune surveillance. *Journal of Medical Signals & Sensors* **9**, 15 (2019). URL http://www.jmssjournal.net/text.asp?2019/9/1/15/253752.

[32] Liao, K.-L., Bai, X.-F. & Friedman, A. Mathematical Modeling of Interleukin-35 Promoting Tumor Growth and Angiogenesis. *PLOS ONE* **9**, e110126 (2014). URL https://journals.plos.org/plosone/article?id=10.1371/journal.pone.0110126. Publisher: Public Library of Science.

[33] Siewe, N. & Friedman, A. TGF-β inhibition can overcome cancer primary resistance to PD-1 blockade: A mathematical model. *PLOS ONE* **16**, e0252620 (2021). URL https://journals.plos.org/plosone/article?id=10.1371/journal.pone.0252620. Publisher: Public Library of Science.

[34] Mukherjee, M. & Levine, H. Cluster size distribution of cells disseminating from a primary tumor. *PLOS Computational Biology* **17**, e1009011 (2021). URL https://journals.plos.org/ploscompbiol/article?id=10.1371/journal.pcbi.1009011. Publisher: Public Library of Science.

[35] Lai, S.-C. A. *et al.* Blocking Short-Form Ron Eliminates Breast Cancer Metastases through Accumulation of Stem-Like CD4+ T Cells That Subvert Immunosuppression. *Cancer Discovery* **11**, 3178–3197 (2021). URL https://cancerdiscovery.aacrjournals.org/content/11/12/3178. Publisher: American Association for Cancer Research Section: Research Articles.

[36] Gui, P. & Bivona, T. G. Evolution of metastasis: new tools and insights. *Trends in Cancer* **0** (2021). URL https://www.cell.com/trends/cancer/abstract/S2405-8033(21)00228-4. Publisher: Elsevier.

[37] Trovato, R. *et al.* The Engagement Between MDSCs and Metastases: Partners in Crime. *Frontiers in Oncology* **10** (2020). URL https://www.frontiersin.org/article/10.3389/fonc.2020.00165.

[38] Laleh, N. G. *et al.* Classical mathematical models for prediction of response to chemotherapy and immunotherapy. *PLOS Computational Biology* **18**, e1009822 (2022). URL https://journals.plos.org/ploscompbiol/article?id=10.1371/journal.pcbi.1009822. Publisher: Public Library of Science.

[39] Wodarz, D. & Komarova, N. *Dynamics Of Cancer: Mathematical Foundations Of Oncology* (World Scientific, 2014).

[40] Pillis, L. G. d., Radunskaya, A. E. & Wiseman, C. L. A Validated Mathematical Model of Cell-Mediated Immune Response to Tumor Growth. *Cancer Research* **65**, 7950–7958 (2005). URL https://cancerres.aacrjournals.org/content/65/17/7950. Publisher: American Association for Cancer Research Section: Immunology.

[41] Rodriguez-Brenes, I. A., Komarova, N. L. & Wodarz, D. Tumor growth dynamics: insights into evolutionary processes. *Trends in Ecology & Evolution* **28**, 597–604 (2013). URL https://www.cell.com/trends/ecology-evolution/abstract/S0169-5347(13)00142-0. Publisher: Elsevier.

[42] Zahir, N., Sun, R., Gallahan, D., Gatenby, R. A. & Curtis, C. Characterizing the ecological and evolutionary dynamics of cancer. *Nature Genetics* **52**, 759–767 (2020). URL https://www.nature.com/articles/s41588-020-0668-4.

[43] Sontag, E. D. A dynamic model of immune responses to antigen presentation predicts different regions of tumor or pathogen elimination. *Cell Systems* **4**, 231–241.e11 (2017). URL https://www.sciencedirect.com/science/article/pii/S2405471216304136.

[44] Sihto, H. *et al.* Breast cancer biological subtypes and protein expression predict for the preferential distant metastasis sites: a nationwide cohort study. *Breast cancer research: BCR* **13**, R87 (2011).

[45] Xiao, W. *et al.* Risk factors and survival outcomes in patients with breast cancer and lung metastasis: a population-based study. *Cancer Medicine* **7**, 922–930 (2018). URL https://onlinelibrary.wiley.com/doi/abs/10.1002/cam4.1370.

[46] Chan, I. S. & Ewald, A. J. The changing role of natural killer cells in cancer metastasis. *The Journal of Clinical Investigation* **132**, e143762 (2022). URL https://www.ncbi.nlm.nih.gov/pmc/articles/PMC8920322/.

[47] Chan, I. S. *et al.* Cancer cells educate natural killer cells to a metastasis-promoting cell state. *The Journal of Cell Biology* **219**, e202001134 (2020).

[48] Øksendal, B. *Stochastic Differential Equations: An Introduction with Applications* (Springer Science & Business Media, 2010).

[49] Fox, R. F. Functional-calculus approach to stochastic differential equations. *Physical Review A* **33**, 467–476 (1986). URL https://link.aps.org/doi/10.1103/PhysRevA.33.467.

[50] Coomer, M. A., Ham, L. & Stumpf, M. P. H. Noise distorts the epigenetic landscape and shapes cell-fate decisions. *Cell Systems* **13**, 83–102.e6 (2022). URL https://www.cell.com/cell-systems/abstract/S2405-4712(21)00339-2.

[51] Wu, C., Hua, Q. & Zheng, L. Generation of Myeloid Cells in Cancer: The Spleen Matters. *Frontiers in Immunology* **11** (2020). URL https://www.frontiersin.org/article/10.3389/fimmu.2020.01126.

[52] Mackey, M. & Glass, L. Oscillation and Chaos in Physiological Control Systems. *Science (New York, N.Y.)* **197**, 287–9 (1977).

[53] Bezanson, J., Edelman, A., Karpinski, S. & Shah, V. B. Julia: A Fresh Approach to Numerical Computing. *SIAM Review* **59**, 65–98 (2017). URL https://epubs.siam.org/doi/10.1137/141000671.

[54] Rackauckas, C. & Nie, Q. Differentialequations.jl–a performant and feature-rich ecosystem for solving differential equations in julia. *Journal of Open Research Software* **5** (2017).

[55] Rackauckas, C. & Nie, Q. Stability-Optimized High Order Methods and Stiffness Detection for Pathwise Stiff Stochastic Differential Equations. In *2020 IEEE High Performance Extreme Computing Conference (HPEC)*, 1–8 (IEEE, Waltham, MA, USA, 2020). URL https://ieeexplore.ieee.org/document/9286178/.

[56] Roesch, E. *et al.* Julia for Biologists. *arXiv:2109.09973 [q-bio]* (2021). URL http://arxiv.org/abs/2109.09973. ArXiv: 2109.09973.

[57] Kuznetsov, V. A., Makalkin, I. A., Taylor, M. A. & Perelson, A. S. Nonlinear dynamics of immunogenic tumors: Parameter estimation and global bifurcation analysis. *Bulletin of Mathematical Biology* **56**, 295–321 (1994). URL https://www.sciencedirect.com/science/article/pii/S0092824005802605.

[58] Diefenbach, A., Jensen, E. R., Jamieson, A. M. & Raulet, D. H. Rae1 and H60 ligands of the NKG2D receptor stimulate tumour immunity. *Nature* **413**, 165–171 (2001).

[59] Apodaca, M. C. *et al.* Characterization of a whole blood assay for quantifying myeloid-derived suppressor cells. *Journal for ImmunoTherapy of Cancer* **7**, 230 (2019). URL https://doi.org/10.1186/s40425-019-0674-1.

[60] Abedi-Valugerdi, M. *et al.* Suppressive effects of low-dose 5-fluorouracil, busulfan or treosulfan on the expansion of circulatory neutrophils and myeloid derived immunosuppressor cells in tumor-bearing mice. *International Immunopharmacology* **40**, 41–49 (2016). URL https://www.sciencedirect.com/science/article/pii/S1567576916303411.

[61] Pillay, J. *et al.* In vivo labeling with 2H2O reveals a human neutrophil lifespan of 5.4 days. *Blood* **116**, 625–627 (2010). URL https://www.sciencedirect.com/science/article/pii/S000649712034708X.

[62] Tak, T., Tesselaar, K., Pillay, J., Borghans, J. A. M. & Koenderman, L. What's your age again? Determination of human neutrophil half-lives revisited. *Journal of Leukocyte Biology* **94**, 595–601 (2013). URL https://onlinelibrary.wiley.com/doi/abs/10.1189/jlb.1112571.

[63] Andrew Yates, R. C. Cell death and the maintenance of immunological memory. *Discrete & Continuous Dynamical Systems - B* **1**, 43–59 (2001).

[64] Lanzavecchia, A. & Sallusto, F. Dynamics of T lymphocyte responses: intermediates, effectors, and memory cells. *Science (New York, N.Y.)* **290**, 92–97 (2000).

[65] Huang, Y. *et al.* CD4 + and CD8 + T cells have opposing roles in breast cancer progression and outcome. *Oncotarget* **6**, 17462–17478 (2015). URL https://www.oncotarget.com/article/3958/text/. Publisher: Impact Journals.

[66] Saltelli, A. A. *Sensitivity analysis in practice : a guide to assessing scientific models* (Chichester ; Hoboken, NJ : Wiley, 2004). URL http://archive.org/details/sensitivityanaly00salt.

[67] Liu, D., Li, L., Rostami-Hodjegan, A., Bois, F. Y. & Jamei, M. Considerations and Caveats when Applying Global Sensitivity Analysis Methods to Physiologically Based Pharmacokinetic Models. *The AAPS Journal* **22**, 93 (2020). URL https://doi.org/10.1208/s12248-020-00480-x.

[68] Therasse, P. *et al.* New Guidelines to Evaluate the Response to Treatment in Solid Tumors. *JNCI: Journal of the National Cancer Institute* **92**, 205–216 (2000). URL https://doi.org/10.1093/jnci/92.3.205.

[69] Spigel, D. R. *et al.* FIR: Efficacy, Safety, and Biomarker Analysis of a Phase II Open-Label Study of Atezolizumab in PD-L1–Selected Patients With NSCLC. *Journal of Thoracic Oncology* **13**, 1733–1742 (2018). URL https://www.jto.org/article/S1556-0864(18)30603-8/fulltext.

[70] Linden, W. v. d., Dose, V. & Toussaint, U. v. *Bayesian Probability Theory: Applications in the Physical Sciences* (Cambridge University Press, Cambridge, 2014). URL https://www.cambridge.org/core/books/bayesian-probability-theory/7C524A165D3EEAEDA68118F1EE7C17F3.

[71] Ge, H., Xu, K. & Ghahramani, Z. Turing: a language for flexible probabilistic inference. In *International Conference on Artificial Intelligence and Statistics, AISTATS 2018, 9-11 April 2018, Playa Blanca, Lanzarote, Canary Islands, Spain*, 1682–1690 (2018). URL http://proceedings.mlr.press/v84/ge18b.html.

[72] Faustino-Rocha, A. *et al.* Estimation of rat mammary tumor volume using caliper and ultrasonography measurements. *Lab Animal* **42**, 217–224 (2013). URL https://www.nature.com/articles/laban.254. Number: 6 Publisher: Nature Publishing Group.

[73] Del Monte, U. Does the cell number 109 still really fit one gram of tumor tissue? *Cell Cycle* **8**, 505–506 (2009). URL https://doi.org/10.4161/cc.8.3.7608. Publisher: Taylor & Francis _eprint: https://doi.org/10.4161/cc.8.3.7608.

[74] Hoffman, M. D. & Gelman, A. The No-U-Turn Sampler: Adaptively Setting Path Lengths in Hamiltonian Monte Carlo. *Journal of Machine Learning Research* **15**, 1593–1623 (2014).

[75] Blaom, A. D. *et al.* MLJ: A Julia package for composable machine learning. *Journal of Open Source Software* **5**, 2704 (2020). URL https://joss.theoj.org/papers/10.21105/joss.02704.

[76] Pedregosa, F. *et al.* Scikit-learn: Machine learning in Python. *Journal of Machine Learning Research* **12**, 2825–2830 (2011).

[77] Hervier, B., Russick, J., Cremer, I. & Vieillard, V. NK Cells in the Human Lungs. *Frontiers in Immunology* **10**, 1263 (2019). URL https://www.ncbi.nlm.nih.gov/pmc/articles/PMC6593268/.

[78] Hu, Z., Li, Z., Ma, Z. & Curtis, C. Multi-cancer analysis of clonality and the timing of systemic spread in paired primary tumors and metastases. *Nature Genetics* **52**, 701–708 (2020). URL https://www.nature.com/articles/s41588-020-0628-z.

[79] Allen, L. J. S. & van den Driessche, P. Relations between deterministic and stochastic thresholds for disease extinction in continuous- and discrete-time infectious disease models. *Mathematical Biosciences* **243**, 99–108 (2013). URL https://www.sciencedirect.com/science/article/pii/S0025556413000527.

[80] Kreger, J., Komarova, N. L. & Wodarz, D. A hybrid stochastic-deterministic approach to explore multiple infection and evolution in HIV. *PLOS Computational Biology* **17**, e1009713 (2021). URL https://journals.plos.org/ploscompbiol/article?id=10.1371/journal.pcbi.1009713. Publisher: Public Library of Science.

[81] Tsimring, L. S. Noise in Biology. *Reports on progress in physics. Physical Society (Great Britain)* **77**, 026601 (2014). URL https://www.ncbi.nlm.nih.gov/pmc/articles/PMC4033672/.

[82] Movahedi, K. *et al.* Identification of discrete tumor-induced myeloid-derived suppressor cell subpopulations with distinct T cell-suppressive activity. *Blood* **111**, 4233–4244 (2008). Place: United States.

[83] Luo, M. C., Nikolopoulou, E. & Gevertz, J. L. From Fitting the Average to Fitting the Individual: A Cautionary Tale for Mathematical Modelers. *Frontiers in Oncology* **12** (2022). URL https://www.frontiersin.org/article/10.3389/fonc.2022.793908.

[84] Laghi, L. *et al.* CD3+ cells at the invasive margin of deeply invading (pT3-T4) colorectal cancer and risk of post-surgical metastasis: a longitudinal study. *The Lancet. Oncology* **10**, 877–884 (2009).

[85] Galon, J. *et al.* Type, density, and location of immune cells within human colorectal tumors predict clinical outcome. *Science (New York, N.Y.)* **313**, 1960–1964 (2006).

[86] Grivennikov, S. I., Greten, F. R. & Karin, M. Immunity, Inflammation, and Cancer. *Cell* **140**, 883–899 (2010). URL https://www.cell.com/cell/abstract/S0092-8674(10)00060-7.

[87] Mantovani, A., Allavena, P., Sica, A. & Balkwill, F. Cancer-related inflammation. *Nature* **454**, 436–444 (2008). URL https://www.nature.com/articles/nature07205.

[88] Swann, J. B. & Smyth, M. J. Immune surveillance of tumors. *The Journal of Clinical Investigation* **117**, 1137–1146 (2007).

[89] Peranzoni, E., Ingangi, V., Masetto, E., Pinton, L. & Marigo, I. Myeloid Cells as Clinical Biomarkers for Immune Checkpoint Blockade. *Frontiers in Immunology* **11** (2020). URL https://www.frontiersin.org/article/10.3389/fimmu.2020.01590.

[90] Bergenfelz, C. *et al.* Systemic monocytic-MDSCs are generated from monocytes and correlate with disease progression in breast cancer patients. *PLoS ONE* **10**, e0127028 (2015). URL https://www.ncbi.nlm.nih.gov/pmc/articles/PMC4439153/.

[91] Benzekry, S. *et al.* Modeling Spontaneous Metastasis following Surgery: An In Vivo-In Silico Approach. *Cancer Research* **76**, 535–547 (2016). URL https://cancerres.aacrjournals.org/content/76/3/535. Publisher: American Association for Cancer Research Section: Integrated Systems and Technologies.

[92] Sahoo, P. *et al.* Mathematical deconvolution of CAR t-cell proliferation and exhaustion from real-time killing assay data. *Journal of The Royal Society Interface* **17**, 20190734 (2020). URL https://royalsocietypublishing.org/doi/full/10.1098/rsif.2019.0734.

[93] Rao, A., Barkley, D., França, G. S. & Yanai, I. Exploring tissue architecture using spatial transcriptomics. *Nature* **596**, 211–220 (2021). URL `https://www.nature.com/articles/s41586-021-03634-9`.

[94] Andersson, A. *et al.* Spatial deconvolution of HER2-positive breast cancer delineates tumor-associated cell type interactions. *Nature Communications* **12**, 6012 (2021). URL `https://www.nature.com/articles/s41467-021-26271-2`.